Geometrical Considerations for Terrain Mapping in SBR Applications

Ke Yong Li, C & P Technologies, Inc., Closter, NJ
Stephen Mangiat, Carnegie Mellon University, Pittsburgh, PA
S. Radhakrishnan Pillai, Ph. D., C & P Technologies, Inc., Closter, NJ
Braham Himed, Ph. D., Air Force Research Laboratory, Rome, NY

Key Words: Space Based Radar, STAP, Terrain Mapping

SUMMARY & CONCLUSIONS

Knowledge aided signal processing calls for the use of existing information such as digitized image maps to further suppress clutter in a typical radar detection operation. In the context of space based radar (SBR) applications, given the SBR parameters and the look angles the first problem is to translate these parameters into a data point on a map. This is realized by converting these parameters into conventional latitude and longitude and then using the corresponding image intensity to estimate the clutter covariance matrix. Using this approach, it is possible to pre-compute the desired weight vector for a location of interest on earth that the SBR is assigned to visit. As a result, using the measured data together with the weight vector, it is possible to test for target detection hypothesis accurately at the time of visit by the SBR.

1. *INTRODUCTION*

An interesting problem in knowledge aided Space Time Adaptive Processing (KA-STAP) is how to make use of traditional image maps to cancel out clutter and interference components while looking for a target. This approach has applications in any 'search and detect' operation including airborne and space based radar (SBR). In what follows we shall illustrate our approach for the SBR applications. The problem in this context is to translate the local geometry to the SBR platform so that the map intensities can be translated into meaningful clutter covariance estimates.

In its general setting two points with respective latitudes and longitudes (α_1, β_1) and (α_2, β_2) are chosen on a map, the first indicating the location of the transmitter/receiver such as an SBR and the second indicating the point of interest (see Fig. 1). In addition, given the SBR height H and its orbit inclination angle η_i at the equator, the first step is to determine all other desired parameters such as SBR elevation angle θ_{EL}, SBR array azimuth angle θ_{AZ}, the true ground range R, grazing angle ψ, the array footprint on earth, range-foldover points $R_1, R_2, \ldots$ on the ground, and finally the correction factor on the azimuth due to the earth's rotation (crab angle) (see Fig. 2 and Fig. 3) [1, 2, 3].

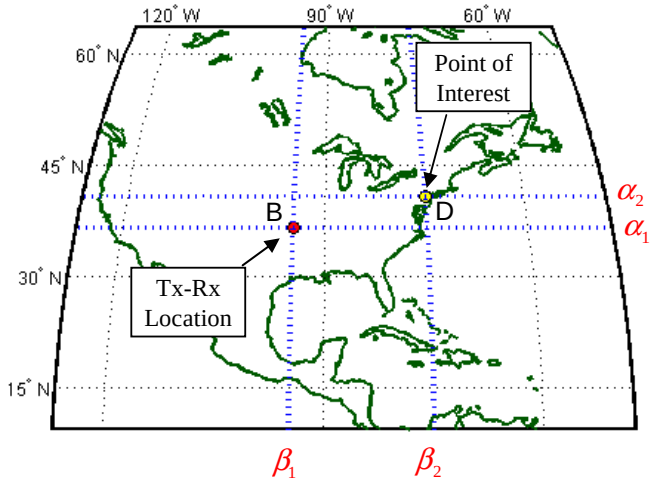

Fig. 1: SBR and point of interest co-ordinates

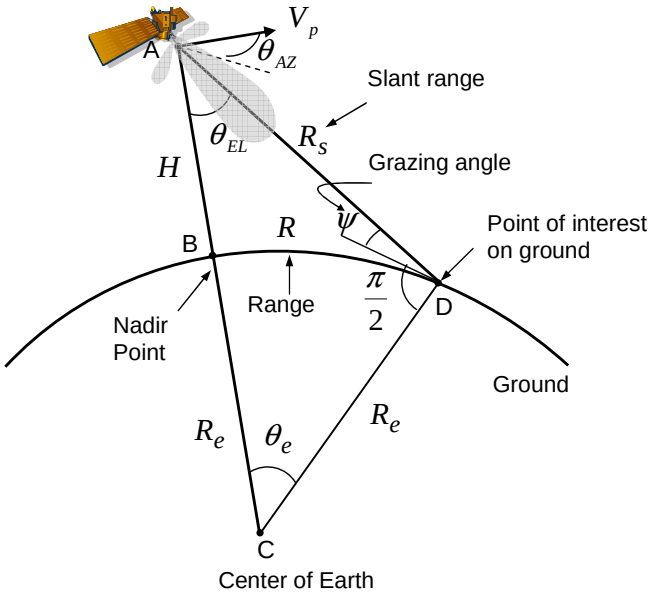

Fig. 2: SBR-Earth Geometry

Report Documentation Page

Form Approved
OMB No. 0704-0188

1. REPORT DATE	2. REPORT TYPE	3. DATES COVERED
01 MAY 2005	**N/A**	**-**

4. TITLE AND SUBTITLE	5a. CONTRACT NUMBER
Geometrical Considerations for Terrain Mapping in SBR Applications	5b. GRANT NUMBER
	5c. PROGRAM ELEMENT NUMBER
6. AUTHOR(S)	5d. PROJECT NUMBER
	5e. TASK NUMBER
	5f. WORK UNIT NUMBER
7. PERFORMING ORGANIZATION NAME(S) AND ADDRESS(ES) **C & P Technologies, Inc., Closter, NJ**	8. PERFORMING ORGANIZATION REPORT NUMBER
9. SPONSORING/MONITORING AGENCY NAME(S) AND ADDRESS(ES)	10. SPONSOR/MONITOR'S ACRONYM(S)
	11. SPONSOR/MONITOR'S REPORT NUMBER(S)

12. DISTRIBUTION/AVAILABILITY STATEMENT
Approved for public release, distribution unlimited

13. SUPPLEMENTARY NOTES
See also ADM002017. Proceedings of the 2005 IEEE International Radar Conference Record Held in Arlington, Virginia on May 9-12, 2005. U.S. Government or Federal Purpose Rights License., The original document contains color images.

14. ABSTRACT

15. SUBJECT TERMS

16. SECURITY CLASSIFICATION OF:			17. LIMITATION OF ABSTRACT	18. NUMBER OF PAGES	19a. NAME OF RESPONSIBLE PERSON
a. REPORT	b. ABSTRACT	c. THIS PAGE			
unclassified	**unclassified**	**unclassified**	**UU**	**6**	

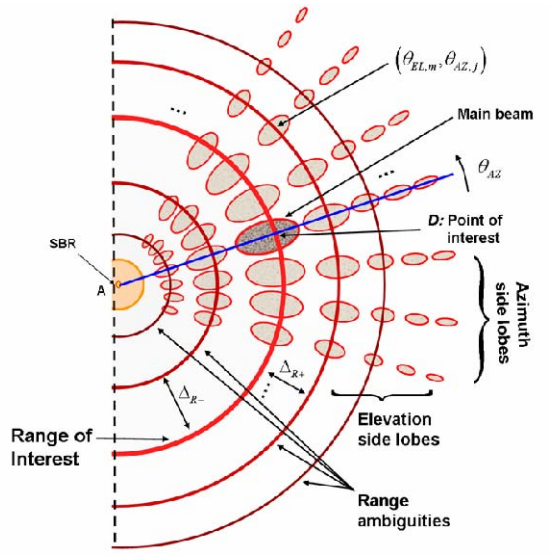

Fig. 3: SBR 2-D Array Gain Pattern and Range Foldovers

The SBR Parameters are listed below (see [4] for derivations):

$$R = R_e \cos^{-1}(\sin\alpha_1 \sin\alpha_2 + \cos\alpha_1 \cos\alpha_2 \cos(\beta_2 - \beta_1)) \quad (1)$$

$$\alpha = \theta_e = R / R_e \quad (2)$$

$$R_s = \sqrt{R_e^2 + (R_e + H)^2 - 2R_e(R_e + H)\cos(R/R_e)} \quad (3)$$

$$\frac{\sin(\pi/2 + \psi)}{(R_e + H)} = \frac{\sin\theta_e}{R_s} = \frac{\sin\theta_{EL}}{R_e} \quad (4)$$

$$\theta_{EL} = \sin^{-1}\left(\frac{R_e}{R_s}\sin(R/R_e)\right) \quad (5)$$

$$\sin\gamma = \cos\alpha_2 \frac{\sin(\beta_2 - \beta_1)}{\sin\alpha} \quad (6)$$

$$\theta_{AZ} = \gamma + \delta - \pi, \quad (7)$$

where

$$\delta = \sin^{-1}\left(\frac{\cos\eta_i}{\cos\alpha_1}\right). \quad (8)$$

These formulas give the SBR parameters in terms of (α_1, β_1), (α_2, β_2), and the SBR height H. Using these parameters the SBR array pattern on the ground can be plotted as shown in Fig. 3. Clearly when pointed at (α_2, β_2) the SBR receives data from all points that are illuminated in Fig. 3, and hence it is necessary to make angular increments both in the elevation and azimuth directions to access the neighbouring points. As a result, it is necessary to develop the inverse formulas when the parameters are appropriately incremented. Such is the case when computing the clutter covariance matrix $\boldsymbol{R}_c$ using an image map.

In general the clutter covariance matrix has the form [1, 2, 3],

$$\boldsymbol{R}_c = \sum_k P_k G(\underline{\theta}_k)\, \boldsymbol{s}(\underline{\theta}_k, \omega_{d_k})\, \boldsymbol{s}^H(\underline{\theta}_k, \omega_{d_k}) \quad (9)$$

where P_k is the intensity of the k^{th} clutter patch, $G(\underline{\theta}_k)$ the corresponding array gain, and $\boldsymbol{s}(\underline{\theta}_k, \omega_{d_k})$ is the space-time steering vector associated with the k^{th} patch. Here $\underline{\theta}_k$ refers to both azimuth angle θ_{AZ_k} and the elevation angle θ_{EL_k} of the point of interest, and in practice are incremented to cover all guard cells used to estimate $\boldsymbol{R}_c$ in (9). In what follows inverse formulas for latitude and longitude, given θ_{EL} and θ_{AZ}, are developed.

2. *AZIMUTH INCREMENT*

From Fig. 4, we have

$$\theta'_{AZ} = \theta_{AZ} + \Delta\theta_{AZ}, \quad (10)$$

where θ_{AZ} and θ'_{AZ} refer to the azimuth angles corresponding to the point of interest before and after the increment, respectively.

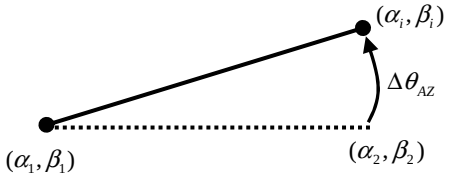

Fig. 4: Azimuth increment

Note that in this case the range remains the same and there is a change in the azimuth angle only. Thus, (7) can be used to compute the new γ.

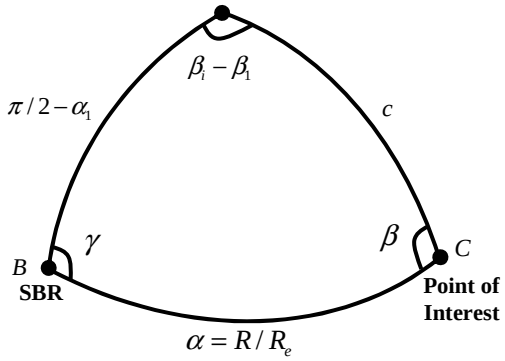

Fig. 5: SBR-point of interest spherical geometry

In the spherical triangle ABC (Fig. 5), two sides and an included angle γ are known. This gives [5]

$$\cos c = \sin\alpha_1 \cos\alpha + \cos\alpha_1 \sin\alpha \cos\gamma \tag{11}$$

and hence the desired latitude of the new point is given by

$$\alpha_i = \pi/2 - c. \tag{12}$$

Once α_i is known, β_i can be obtained from the relation [5]

$$\frac{\sin(\beta_i - \beta_1)}{\sin\alpha} = \frac{\sin\gamma}{\sin c}. \tag{13}$$

3. *ELEVATION INCREMENT*

In this case the new elevation angle corresponding to the point of interest is given by (see Fig. 6)

$$\theta'_{EL} = \theta_{EL} + \Delta\theta_{EL}, \tag{14}$$

where θ_{EL} refers to the elevation angle before the increment.

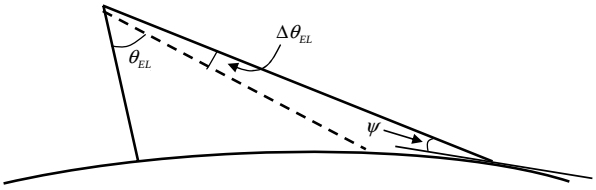

Fig. 6: Elevation increment

With the incremented value of the elevation angle, Eq. (4) can be used to determine the grazing angle ψ. Thus,

$$\psi = \cos^{-1}\left(\frac{\sin\theta_{EL}}{1 + H/R_e}\right) \tag{15}$$

and the relation

$$\theta_e = \pi/2 - \theta_{EL} - \psi \tag{16}$$

can be used to determine the new range R. This gives

$$R = R_e\theta_e = R_e(\pi/2 - \theta_{EL} - \psi). \tag{17}$$

Note that θ_{AZ} and γ remain unchanged and (11) – (13) can be used to compute (α_i, β_i). Knowing the latitude and longitude, the power level can be extracted from the map. This procedure is repeated to cover all guard cells of interest in (9).

Another refinement in modelling the clutter covariance matrix is to introduce the effect of range foldover ambiguities into (9). Range foldover occurs when clutter returns from previously transmitted pulses are coherently combined with the mainbeam at the point of interest, as shown in Fig. 7. The associated range points corresponding to these returns constitute the range ambiguities for the point of interest.

4. *RANGE FOLDOVER*

The ground plane resolution of the SBR is limited by the pulse frequency and the grazing angle ψ. This causes range ambiguities spaced at the limiting resolution δ_R, given by

$$\delta_R = \frac{cT}{2}\sec\psi. \tag{18}$$

From (18) and for short range regions where the grazing angle ψ is closer to $\pi/2$, the range resolution is very poor since $\delta_R \to \infty$. For long ranges, the resolution approaches its limiting value $cT/2$ as $\psi \to 0$.

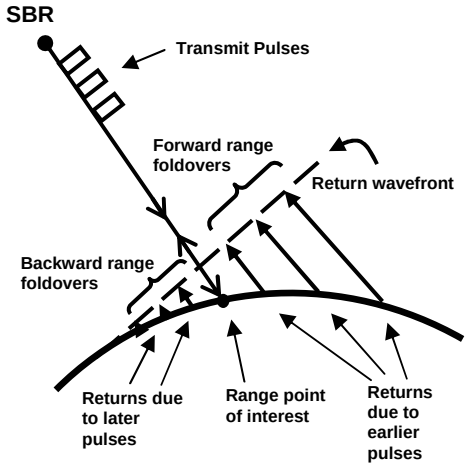

Fig. 7: Range Foldover

If R_s represents the slant range at the end of one pulse, then $R_s + cT/2$ is the new slant range at the end of the next pulse. Let $R + \Delta_R$ represent the new range corresponding to the second pulse shadow on the ground. Using Fig. 2, we have

$$(R_s + cT_r/2)^2 = R_e^2 + (R_e + H)^2 - 2R_e(R_e + H)\cos\left(\frac{R + \Delta_R}{R_e}\right) \tag{19}$$

or

$$\Delta_R = R_e \cos^{-1}\left(\frac{R_e^2 + (R_e + H)^2 - (R_s + cT/2)^2}{2R_e(R_e + H)}\right) - R. \tag{20}$$

Note that Δ_R is a decreasing function of R. Moreover when R is relatively small, the distance between the pulse shadows on the ground is large and it decreases as R increases. However for large values of range, Δ_R remains constant at its limiting value $cT_r/2$. As a result and as the range increases,

this has the additional effect of packing several range ambiguities within a mainbeam footprint.

If we assume Δ_R to be constant within a mainbeam footprint, then the number of range ambiguities within the mainbeam is given by

$$N_a = (R_T - R_H)/\Delta_R. \tag{21}$$

Otherwise, starting at the heel of the mainbeam located at range R_H, $\Delta_{R_1}, \Delta_{R_2}, \cdots$, are sequentially calculated with the mainbeam footprint until the toe is reached. Thus, the number of range ambiguities N_a within a mainbeam satisfies the equation

$$\Delta_{R_1} + \Delta_{R_2} + \cdots + \Delta_{R_{Na}} = R_T - R_H . \tag{22}$$

Each range ambiguity contribution to the clutter covariance matrix has the same form as in (9). As a result, the clutter covariance matrix that accounts for range ambiguities has the following form

$$\boldsymbol{R}_c = \sum_{m=0}^{N_a} \sum_{k} P_{km}\, G(\underline{\theta}_{km})\, \boldsymbol{s}(\underline{\theta}_{km}, \omega_{d_{km}})\, \boldsymbol{s}^H(\underline{\theta}_{km}, \omega_{d_{km}}) . \tag{23}$$

Here $P_{k,m}$ corresponds to the intensity of the k^{th} patch from the m^{th} range foldover. For each range ambiguity in (23), the azimuth increment method described earlier can be applied to compute its clutter covariance matrix contribution.

Finally the clutter Doppler $\omega_{d_{km}}$ in (23) can be modelled with and without taking earth's rotation into account. The effect of earth's rotation tends to modify the clutter Doppler in terms of a crab angle ϕ_c and a crab magnitude ρ_c affecting its phase and magnitude [2, 3]. With T representing the transmit pulse period and V_p the satellite velocity, it can be shown that the clutter Doppler with earth's rotation for the k^{th} patch is given by [2, 3]

$$\omega_{d_{km}} = \frac{2V_p T}{\lambda/2} \rho_c \sin\theta_{EL_k} \cos(\theta_{AZ_m} + \phi_c) . \tag{24}$$

5. *TERRAIN MAPPING*

Using the method described above to update the latitude and longitude, terrain data from any stand alone image map can be used to custom compute the covariance matrix. For illustration purposes, we have used image intensity data from a world map at http://www.cs.brown.edu/exploratories.

Fig. 8 shows the SBR coverage for two regions, (i) the eastern United States ($\alpha_1 = 34^o$, $\beta_1 = -100^o$) and (ii) the Middle East. To compute the clutter covariance matrix for each region, the array patterns and the range foldovers are projected on the surface of the earth using (10)-(17). In addition, the range foldovers are included in this case since we are using a pulse repetition frequency of 500 Hz. For an SBR at a height of 506 km, we have $R_{\max} \approx 2400$ km and N_a is equal to 6 or 7 depending on the target range. By carrying out the latitude/longitude – azimuth/elevation conversion, the terrain of interest can be superimposed on an image map to obtain the true terrain image intensities. These intensity values P_{ik} together with the terrain geometry described earlier can be used to estimate the clutter covariance matrix $\boldsymbol{R}_c$ for the point of interest with elevation and azimuth angles θ_{EL_O} and θ_{AZ_O}. Knowing the SBR array/pulse configuration, if $\boldsymbol{s}(\underline{\theta}_o, \omega_d)$ represents the space-time steering vector for the target location, then

$$\boldsymbol{w} = \boldsymbol{R}_c^{-1} \boldsymbol{s}(\underline{\theta}_o, \omega_d) \tag{25}$$

represents the desired weight vector that can be applied to a data sample to determine the presence or absence of a target of interest.

Fig. 9 shows the performance of the optimum weight vector in terms of its ability to perform clutter suppression with and without the presence of range foldover using the Signal to Interference plus Noise (SINR) measure, given by

$$SINR = \boldsymbol{s}^H(\underline{\theta}_o, \omega_d)\, \boldsymbol{R}_c^{-1}\, \boldsymbol{s}(\underline{\theta}_o, \omega_d) . \tag{26}$$

Their combined effect results in appreciable performance degradation as shown in Fig. 9. In this context, the presented approach gives a tool to evaluate the performance degradation at various points on earth. A preliminary simulation shows the clutter suppression for different points of interest across the United States.

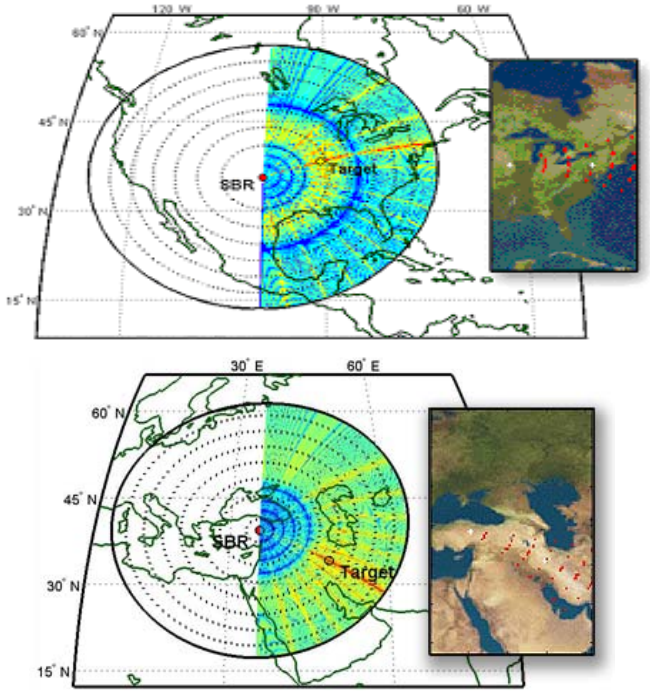

Fig. 8: SBR coverage and range foldover maps. Attached images are used to estimate the clutter covariance matrix.

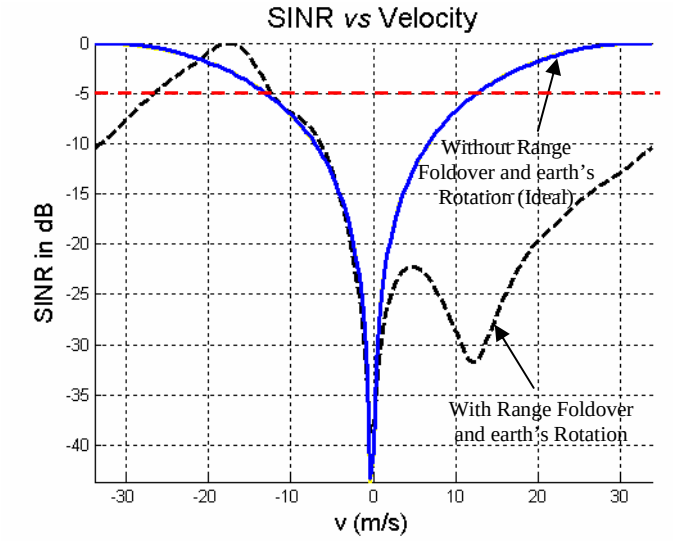

Fig. 9: MDV performance with and without Range Foldover and Crab Angle (Range = 1200km, Azimuth = 88°)

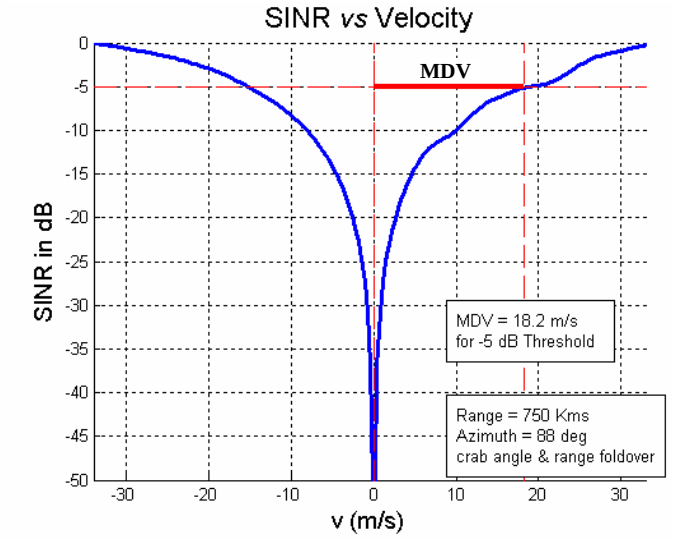

Fig. 10: Minimum Detectable Velocity for -5 dB threshold.

6. *EFFECTS OF TERRAIN ON CLUTTER SIMULATION*

As previously described, the intensities obtained from an image map can be used when estimating the clutter covariance matrix, $\boldsymbol{R}_c$. To test these effects, multiple simulations were run at different points over the United States within the three regions of interest as shown in Fig. 11. First, the target range and azimuth angle were held constant at 900 km and 88° and the location of the SBR was moved among the three longitudes (-125°, -110°, -95°) and four latitudes (36°, 38°, 40°, 42°). By making use of (23)-(26) the clutter suppression performance at each of these locations can be studied using the output SINR. The results are shown in terms of the Minimum Detectable Velocity (MDV) measure for ground moving target detection. From Fig. 10 MDV is a measure of the ability to detect slow moving targets in the presence of clutter and noise. From there, clearly a sharp clutter ridge provides superior performance. For the sake of comparison, we have set the threshold for MDV at 5 dB below the noise floor as shown in Figs. 9-10. Notice that when earth's rotation is present MDV is undefined as shown in Fig. 9, indicating the a severe degradation in performance.

The average MDV values for the three regions are shown in Fig. 11. The MDV variations at different latitudes within each region are shown in Fig. 12. Notice that the Midwest region gave an average MDV of 23.2749 m/s whereas the West region gave an average MDV of 24.3179 m/s (See Fig. 11). The East region MDV was also slightly higher than the Midwest. The Midwest is generally flatter and more uniform than the other regions so one would expect lower MDV's due to the "homogeneous" nature of the background terrain.

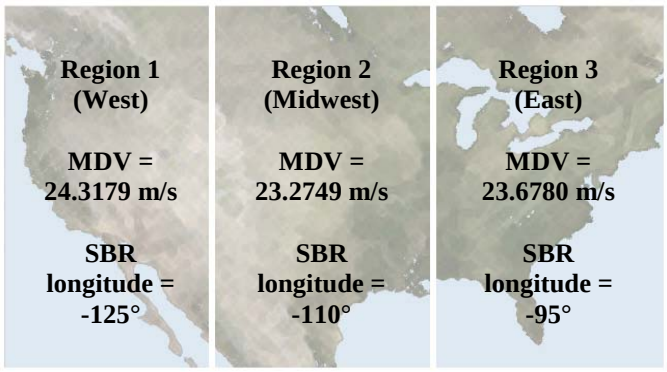

Fig 11: Regions used for Terrain Mapping.

Similarly, we repeated the above simulations while keeping the latitude constant at 40° and adjusting the azimuth around 90° (See Fig.13). In this case, MDV increase above the other regions for the Midwest at larger azimuth angles. This could be due to terrain variations such as the southern end of the Rocky Mountains and the Gulf of Mexico. Yet as before, MDV values for the Midwest are lower when the beam covered the plains.

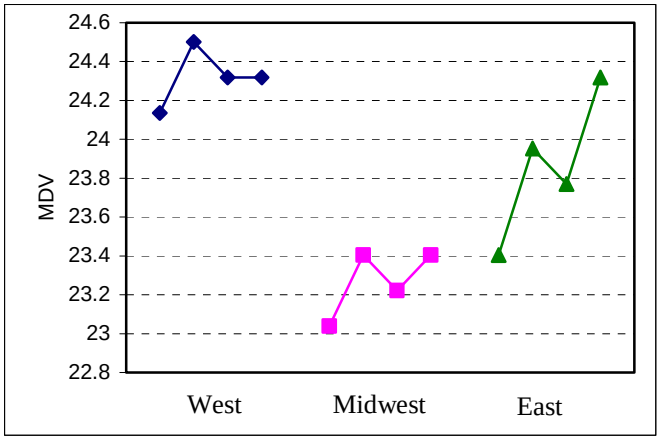

Fig. 12: Range = 800km, Azimuth = 88°
MDV calculated at four latitudes in each region.

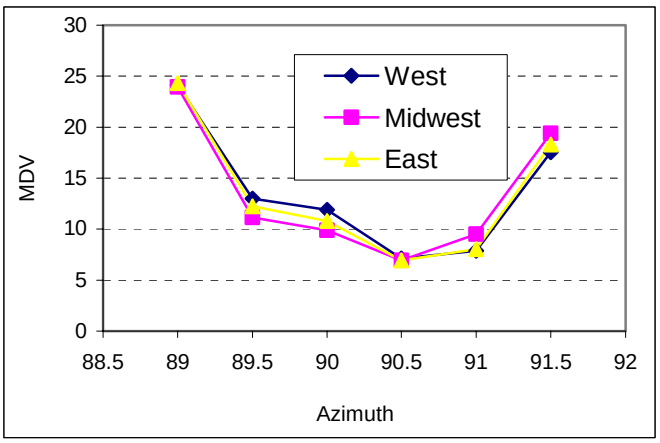

Fig. 13: Range = 800km, latitude = 40°. MDV calculated for different azimuth in each region.

7. *CONCLUSIONS*

This paper discusses methods for incorporating existing digital maps using SBR-earth geometry to generate realistic clutter covariance nulling schemes for ground moving target detection applications. SBR-earth geometry parameters need to be updated into the latitude-longitude scale to determine the actual image intensities. This approach allows pre-computed optimum weight vectors to be determined that can be used on a single snapshot of measurement to determine the presence or absence of a target. Performance results using this approach across the United States terrain are reported in terms of Minimum Detectable Velocity (MDV) and indicate the clutter suppression efficiency.

ACKNOWLEDGEMENTS

Research reported here partially supported under Rome AFRL SBIR Phase II contract FA8750-04-C-0202.

REFERENCES

1. Peter Zulch, Mark Davis, Larry Adzima, Robert Hancock and Sid Theis, "The Earth Rotation Effect on a LEO L-Band GMTI SBR and Mitigation Strategies", *IEEE Radar Conference*, Philadelphia, PA, April 2004.
2. S. U. Pillai, B. Himed, K. Y. Li, "Waveform Diversity for Space Based Radar", *Proc. of Waveform Diversity and Design*, Edinburgh, Scotland, Nov 8-10, 2004.
3. S. U. Pillai, B. Himed, K. Y. Li, "Modeling Earth's Rotation for Space Based Radar", *Asilomar Conference on Signals, Systems*, Asilomar, CA, Nov 7-10, 2004.
4. K. Y. Li *et. al*., "STAP for Space Based Radar," *Air Force Research Laboratory Final Technical Report*, AFRL-SN-RS-TR-2004-170, June, 2004.
5. W. M. Smart, Text Book on Spherical Astronomy, Cambridge University Press, Cambridge, 1965.

BIOGRAPHIES

Ke Yong Li is a staff engineer with C & P Technologies, Inc., New Jersey specializing in radar signal processing. His research interest includes Space Time Adaptive Processing (STAP), Optimum Trans-Receiver design technology and space based radar signal processing.

Stephen V. Mangiat is a engineering student-intern of C & P Technologies, Inc. He will receive the bachelors' degree in electrical and computer engineering from Carnegie Mellon University in June 2005. He has developed Java Applets to illustrate blind echo cancellation algorithms and graphical user interface application for Space Based Radar clutter simulation.

S. Radhakrishnan Pillai is a senior engineer with C & P Technologies, Inc, New Jersey. His research interest includes space-time adaptive processing (STAP) and waveform diversity for radar and communication applications.

Braham Himed is a senior research engineer with the United States Air Force Research Laboratory, Sensors Directorate. His research interests include detection, estimation, multichannel adaptive signal processing, time series analyses, array processing, space-time adaptive processing, hot clutter mitigation, and ground penetrating radar technology.